Reactions of Methyl Viologen Dication (MV^{2+}) with H Atoms in Aqueous Solution: Mechanism Derived from Pulse Radiolysis Measurements and ab Initio MO Calculations

Tomi Nath Das,* Tapan K. Ghanty,[§] and Haridas Pal[†]

Radiation Chemistry & Chemical Dynamics Division, Bhabha Atomic Research Centre (B.A.R.C.), Trombay, Mumbai 400 085, India

Received: December 17, 2002

The mechanistic details of a H atom ($H^{\bullet}$ radical) reaction with the methyl viologen (Paraquat) dication, MV^{2+}, in aqueous solutions is presented, based on pulse radiolysis measurements in acid ($HClO_4$) solution and supported by ab initio molecular orbital calculations. H atom-initiated reduction follows three different paths. About 76% of reactions follow the H atom addition to one of the ring C atom positioned meta to a N atom. The resulting cyclohexadienyl-type radical ($MVH_C^{\bullet 2+}$) shows an absorption peak at 350 nm (fwhm = 40 nm, $\epsilon = 4470 \pm 300\ M^{-1}\ cm^{-1}$), and its second-order decay rate ($2k_{350nm} = 2.6 \pm 1.1 \times 10^9\ M^{-1}\ s^{-1}$) suggests a radical−radical disproportionation reaction. About 10% of H atom reactions proceed with abstraction of one H atom from a $>N-CH_3$ group, resulting in the formation of a $>N-CH_2^{\bullet}$ radical. Subsequently, its transformation into the *N*-hydroxycyclohexadienyl-type radical ($MVOH_N^{\bullet 2+}$) in the presence of water is indicated. The $MVOH_N^{\bullet 2+}$ radical is exclusively generated during the $^{\bullet}OH$ radical reaction with MV^{2+}. It shows two absorption peaks at 315 nm (fwhm = 45 nm, $\epsilon = 7400 \pm 400\ M^{-1}\ cm^{-1}$) and 470 nm (fwhm = 60 nm, $\epsilon = 15\,300 \pm 700\ M^{-1}\ cm^{-1}$); a mixed-order radical decay in this case suggests a complex kinetics. The remaining H atom reaction proceeds with an H adduct formation at one of the two N atoms. The resulting $MVH_N^{\bullet 2+}$ radical shows a pK_a value of -0.2 ± 0.1 corresponding to the $MVH_N^{\bullet 2+} + H_2O \leftrightarrow MV^{\bullet +} + H_3O^+$ equilibrium. Thus, in solution of pH > 1, deprotonation of the $MVH_N^{\bullet 2+}$ radical results in the appearance of the well-known intense blue $MV^{\bullet +}$ radical absorption signal ($\lambda_{max} = 393$ nm, $\epsilon = 42000 \pm 1200\ M^{-1}\ cm^{-1}$; $\lambda_{max} = 605$ nm, $\epsilon = 13\,300 \pm 550\ M^{-1}\ cm^{-1}$), also obtained directly during MV^{2+} reduction by e_{aq}^-, $CO_2^{\bullet -}$, etc. These results also reconfirm that a previous report of the pK_a value of 2.9 for $MVH^{\bullet 2+}$ adduct radical was merely a reflection of e_{aq}^- scavenging in acidic solution.

Introduction

Methyl viologen (Paraquat, Scheme 1) commonly exists as the MV^{2+} dication salt with either $2Cl^-$ or SO_4^{2-} as the counterion. MV^{2+} is known for its diverse applications, such as an herbicidal and toxicological agent,[1−3] an electron acceptor and transfer catalyst in redox reactions,[4,5] a reference-reducing radical in different matrixes,[6] an electron-accepting agent in photochemical and photoelectrochemical devices aiming to harness solar energy,[7] and in devising electrochromic display systems.[8,9] Use of MV^{2+} in these areas becomes feasible mainly because of its facile one-electron reduction to the blue radical cation $MV^{\bullet +}$ by a suitable reducing agent (R), reaction 1, and subsequent participation of this latter intermediate in various applications.

$$MV^{2+} + R \rightarrow MV^{\bullet +} + R^{\bullet +} \qquad (1)$$

In the family of free-radical reductants, the H atom ($H^{\bullet}$ radical) is also considered to be a strong reducing agent,[10] and its formation or presence in the above photo, thermal, and electric discharge and radiation-induced reactions in the presence of H_2O/H_3O^+ and H_2 in different phases are now well established.[6,11] However, the H atom reactions are not known to follow the general outer-sphere electron-transfer mechanism (reaction 1).[6] Therefore, a quantitative mapping of a H atom reaction with MV^{2+} would not only necessitate a prior knowledge of its presence but also suitable incorporation of its specific reaction(s) with MV^{2+}. Although aqueous medium remains the natural choice for such studies, available details in the literature are not satisfactory, mainly because under the insufficiently acidic conditions employed therein,[12a,b] the simultaneous presence of e_{aq}^- and its reactions to generate the radical cation $MV^{\bullet +}$ (reaction 1) could not be avoided because of a high rate constant (reported k_1 for $e_{aq}^- = 5.4-9.0 \times 10^{10}\ M^{-1}\ s^{-1}$).[6] Additionally, the presence of the $MV^{\bullet +}$ radical also imposed a major experimental challenge in characterizing any other transient radical because of its intense and broad absorption bands in the UV−vis range ($\epsilon_{390-396nm} = 33\,000-45\,000\ M^{-1}\ cm^{-1}$; $\epsilon_{600-605nm} = 8000-14\,000\ M^{-1}\ cm^{-1}$).[13−16]

In case of the H atom, the following processes also add to the complexity of the reactions. In highly alkaline pH though, the H atom gets deprotonated following reaction 2 and, consequently, the e_{aq}^- reactions may gain prominence. At a low pH, on the other hand, protonation reaction 3 may change the initiating radical nature and the subsequent reaction mechanism.

$$H^{\bullet} + OH^- \rightarrow e_{aq}^- \ (k = 2.2 \times 10^7\ M^{-1}\ s^{-1}) \qquad (2)$$

$$e_{aq}^- + H_3O^+ \rightarrow H^{\bullet} \ (k = 2.3 \times 10^{10}\ M^{-1}\ s^{-1}) \qquad (3)$$

Furthermore, the reaction intermediates arising out of the H atom/e_{aq}^- addition may also be interrelated by a deprotonation equilibrium. Thus, transient characterization needs to take into consideration all these interfering effects.

* Author to whom correspondence should be addressed. E-mail: tndas@apsara.barc.ernet.in.

[§] E-mail: tapang@apsara.barc.ernet.in.

[†] E-mail: hpal@apsara.barc.ernet.in.

10.1021/jp022614r CCC: $25.00
Published on Web 07/15/2003

SCHEME 1

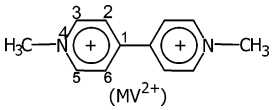

The electrophilic nature of the H atom addition suggests its natural preference for the MV^{2+} ring. However, it can also abstract an H atom from the sp^3 carbon of a methyl group, producing a C-centered radical and H_2.[6] With four dissimilar sites available for H atom addition (i.e., atoms C1, C2, C3, and N4 in Scheme 1, all other positions being equivalent), each of these adduct formations would result in the ring host-atom hybridization to change from sp^2 to sp^3, destroying the planarity and electronic conjugation in the concerned ring to different extents. Even the fifth $>N-CH_2^{\bullet}$ radical site, arising out of the H atom abstraction reaction, would be only partially resonance-stabilized because of reduced conjugation as compared to the $MV^{\bullet+}$ radical.[17−19] To unmask the interfering effects of the $MV^{\bullet+}$ radical and establish the MV^{2+} + H atom reaction mechanism, our approach in this study has been as follows. First, we have conveniently generated the H atom quantitatively (in the absence of e_{aq}^-) employing pulse radiolysis (PR) experiments in highly acidic solutions.[20a] Second, taking assistance from ab initio molecular orbital (MO) calculations describing the molecular structure, electron-density, and spin-density mappings,[21] we have systematically compared all the different $H^{\bullet} + MV^{2+}$ reaction transient properties to judge their actual experimental occurrence and arrive at the overall reaction mechanism. Our results indicate major differences in the initiation step for the H atom reaction with MV^{2+} as compared to the simple electron transfer in reaction 1.

Experimental Section

Materials and Procedure. All the solutions were prepared in triple-distilled water. The gases O_2, N_2, and N_2O used for purging these solutions were obtained locally from British Oxygen Ltd. (purity ∼99.95%). Methyl viologen dichloride trihydrate obtained from Aldrich was of 98% purity, and upon comparing its spectrum with the published values,[14] further purification was found unnecessary. Other chemicals, such as *tert*-butyl alcohol, KOH, KCl, HCO_2Na, HCO_2H, and $HClO_4$ (60 wt %), were of the highest purity available locally from SD Fine Chemicals and used as received. All PR measurements were made at ambient temperatures close to 26 ± 1 °C. All spectral measurements were made on a Hitachi 330 spectrophotometer.

The 7 MeV electron-pulse radiolysis kinetic spectrophotometric detection setup used in this study has been described in detail before.[22,23] Samples were irradiated in a 1 × 1 cm^2 Suprasil cell. Optical detection of transients was performed within the spectral range of 230−800 nm using a 450 W xenon lamp and a Kratos monochromator blazed at 300 nm coupled to a Hamamatsu R-955 photomultiplier tube. A spectral resolution of ∼3 nm was routinely achieved, and the background of scattered light at 250 nm was <2%. Sample replenishment before each pulse was achieved with the help of a flow arrangement, and oscilloscope traces were averaged during spectral and kinetic measurements. For dosimetry, a 0.01 M aerated SCN^- solution was used, taking its $G = 0.34$ μmol J^{-1} and the $G{\cdot}\epsilon = 2.59 \times 10^{-4}$ m^2 J^{-1} at 475 nm.[24] The general uncertainty of ±15% in results from the PR experiments relates to all subsequent measurements.

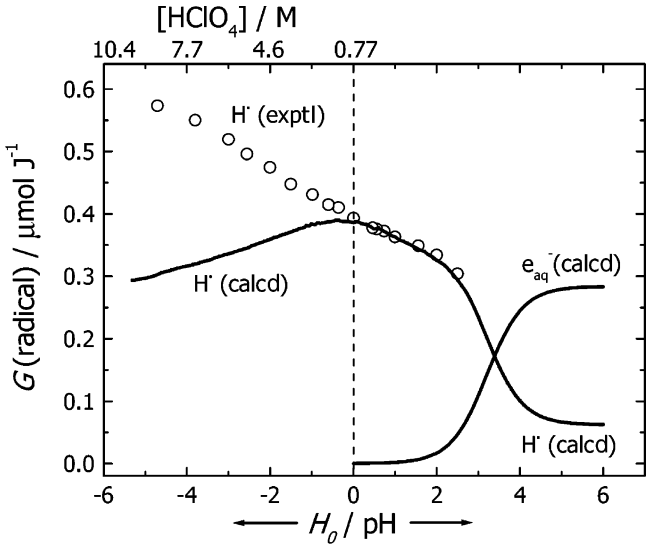

Figure 1. Yield of reducing radicals $H^{\bullet}$ and e_{aq}^- in aqueous $HClO_4$ solution.

Results and Discussion

Yield of H Atom in Acid. During radiolysis in dilute aqueous solutions, various primary reducing and oxidizing radicals were homogeneously distributed within ∼10^{-7} s (reaction 4), with their after-pulse yields G (in μmol J^{-1}) shown in parentheses.[25]

$$H_2O \rightsquigarrow {}^{\bullet}OH\ (0.28),\ H^{\bullet}\ (0.062),\ e_{aq}^-\ (0.28)\ etc \qquad (4)$$

In general, with increasing acidity (below pH 3.5), competition from reaction 3 changes the available e_{aq}^- to a H atom ratio for reaction with a dissolved solute (in submillimolar concentration range). However, in the presence of ca. 200 μM MV^{2+} (a working concentration), subsequent formation of $MV^{\bullet+}$ following reaction 1 can be prevented only at pH ≤ 1.0 because of an exceptionally high k_1 value. Thus, for a true evaluation of H atom reaction alone (i.e., in the absence of any direct e_{aq}^- effect) an even higher solution acidity (with $HClO_4$ in molar quantities) is desirable, and in such cases of high acidity (below pH 0), the overlapping H_0 scale needs to be evoked.[26] Radiolysis schemes of a few molar $HClO_4$ solutions from a recent study[20a] allows a qualitative calculation of $G(H^{\bullet})$ in such cases. In Figure 1, the calculated $G(H^{\bullet})$ vs H_0/pH plot covering an acidity range represented by H_0 −5.0 to pH 6 is shown by the continuous curves $H^{\bullet}$ (calcd). These calculations are based on the principle of radiation energy partition between the two solvent components H_2O and $HClO_4$, taking into account the accepted valence electron fraction methodology.[27] (The results from the less-used total-electron fraction methodology is not presented here; those values were marginally higher). However, in the presence of molar quantities of $HClO_4$, scavenging/trapping of quasi-dry electrons even in a subpicosecond time scale by H_3O^+ is reported to lead to a still-higher value for the H atom yield.[20b] To have an experimental measure of this desired parameter in the high acidity range, N_2-saturated 150 μM biphenyl (BP) solution was irradiated (with a 10 Gy dose) in the presence of 0.4 M *tert*-butyl alcohol (to scavenge all the oxidizing radicals, i.e., $^{\bullet}OH$, $ClO_3^{\bullet}$, and $ClO_4^{\bullet}$). The adduct $BPH^{\bullet}$ radical was formed by reaction 5.

$$BP + H^{\bullet} \rightarrow BPH^{\bullet} \qquad (5)$$

Matching radical spectral profiles at H_0 −4.8 and pH 2 confirmed that the nature of this adduct remained unchanged

even in the presence of high $HClO_4$ concentration. Taking $BPH^{\bullet}$ radical ϵ_{360nm} value = 5000 M^{-1} cm^{-1} for its absorption peak,[28] the experimental $G(H^{\bullet})$ values were estimated taking ≥90% of the H atom reaction with BP under these conditions. The remaining H atoms were lost in reactions with *tert*-butyl alcohol (and also in its radical-dimerization reactions).[6] These data are plotted in Figure 1 as $H^{\bullet}$ (exptl). Although the $H^{\bullet}$ (exptl) and $H^{\bullet}$ (calcd) values match above pH 0, their increasing divergence with decreasing H_0 provides the estimate for electron scavenging/trapping at high acidity (a_{H3O+}). In all subsequent measurements, the $H^{\bullet}$ (exptl) values were used to normalize the transient yields from H atom reactions. In Figure 1, the $G(e_{aq}^{-})$ values are plotted as e_{aq}^{-} (calcd) to show the correlation between the after-pulse yields of $H^{\bullet}$ and the e_{aq}^{-} radicals at pH > 0.

Absorption Characteristic of $MV^{\bullet+}$ Radicals. To check the parent MV^{2+} stability in our working H_0/pH range, its absorption characteristics at neutral pH were compared with H_0 −4 and pH 14 solutions. These resulting profiles with λ_{max} = 258 nm and ϵ = 23 000 M^{-1} cm^{-1} were found to remain unchanged even under these extreme conditions. Since all the spectral evaluations of the present work were intended to be made after taking into account any contribution from the $MV^{\bullet+}$ radical absorption, fresh spectral measurements were made for the latter. The $MV^{\bullet+}$ radicals in these measurements were exclusively generated via (i) reaction of MV^{2+} with e_{aq}^{-} in N_2-saturated solution containing 0.5 M *tert*-butyl alcohol near neutral pH and pH ∼14 (in the latter case, for long use it was found necessary to flow MV^{2+} and KOH solutions in different channels and later mix these prior to irradiation by using the mixer assembly described in our earlier study[23]) and (ii) electron transfer from the $CO_2^{\bullet-}$ radical to MV^{2+}. In case of the e_{aq}^{-} reaction, high reactivity of reaction 2 at pH 14 (∼2.2 × 10^7 s^{-1}) ensured negligible interference from the H atom (at [MV^{2+}] = 200 μM, H atom reactivity remained ≤10^5 s^{-1}). Interference due to $^{\bullet}OH/^{\bullet}O^{-}$ radicals was minimized by the *tert*-butyl alcohol present, and the resulting β-hydroxy radical ($^{\bullet}CH_2(CH_3)_2COH$) from the $^{\bullet}OH/^{\bullet}O^{-}$ + $(CH_3)_3COH$ reaction[25,29,30] was found to have negligible reactivity toward MV^{2+}. This approach to scavenge the $^{\bullet}OH/^{\bullet}O^{-}$ radicals was also adopted earlier by Solar et al.[12a] For the $CO_2^{\bullet-}$ radical reaction, the spectral measurements were made at a few selected pHs with 200 μM MV^{2+} and using either N_2O-saturated 50−500 mM HCO_2Na solution at pH > 4 or N_2-saturated ∼1.0 M HCO_2H/HCO_2^{-} solution at pH < 2. In addition to reaction 3, the following sequence of reactions 6−10 (along with some direct e_{aq}^{-} + MV^{2+} reaction 1) ensured formation of only the $MV^{\bullet+}$ radical.

$$e_{aq}^{-} + N_2O \rightarrow N_2 + {}^{\bullet}O^{-} \quad (k = 9.1 \times 10^9\ M^{-1}\ s^{-1}) \qquad (6)$$

$$^{\bullet}O^{-} + H_2O \leftrightarrow OH^{-} + {}^{\bullet}OH \quad (k_f = 9.4 \times 10^7\ s^{-1},\ k_r = 1.3 \times 10^{10}\ M^{-1}\ s^{-1}) \qquad (7)$$

$$H^{\bullet} + HCO_2^{-}/HCO_2H \rightarrow CO_2^{\bullet-} + H_2 \quad (k = 2100/4.4 \times 10^5\ M^{-1}\ s^{-1}) \qquad (8)$$

$$^{\bullet}OH + HCO_2^{-}/HCO_2H \rightarrow CO_2^{\bullet-} + H_2O \quad (k = 32.0/1.8 \times 10^8\ M^{-1}\ s^{-1}) \qquad (9)$$

$$CO_2^{\bullet-} + MV^{2+} \rightarrow CO_2 + MV^{\bullet+} \quad (k = 6.4 \times 10^9\ M^{-1}\ s^{-1}) \qquad (10)$$

Few transient absorption spectra from these measurements are shown in Figure 2. These spectra (λ_{max} = 393 nm, ϵ = 42 000 ± 1200 M^{-1} cm^{-1} and λ_{max} = 605 nm, ϵ = 13 300 ± 550 M^{-1} cm^{-1}) match well with the reported profile of the $MV^{\bullet+}$ radical from earlier studies.[12−15] From the spectral profiles in Figure 2, various ratios of A_λ/A_{393} at selected wavelengths (λ) were used for later comparisons with other spectral profiles measured in this study. With the $CO_2^{\bullet-}$ radical, these measurements could be extended up to pH 0.9 because of the corresponding (protonated) radical, $HCO_2^{\bullet}$ (pK_a value −0.2).[31] However, below pH 0.5, the $CO_2^{\bullet-}$ radical yield decreased rapidly because of lower propensity of its generation by $H^{\bullet}/^{\bullet}OH$ radicals from HCO_2H, as compared to HCO_2^{-} at higher pH (pK_a of HCO_2H = 1.8).[25]

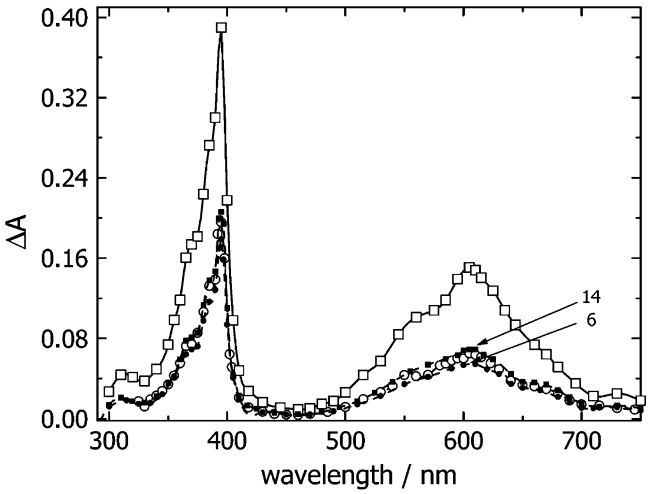

Figure 2. Transient $MV^{\bullet+}$ absorption spectra for 200 μM MV^{2+} with (a) $CO_2^{\bullet-}$ radical in the presence of 1.0 M (total of) HCO_2H and HCO_2^{-} under N_2 saturation; pH 0.9; dose 14.3 Gy; ΔA_{max} ([radical] = 9.3 μM) 6.3 μs after pulse (-□-); (b) $CO_2^{\bullet-}$ radical in the presence of 65 mM HCO_2^{-} under N_2O saturation; pH 8; dose 7.5 Gy; ([radical] = 4.9 μM) 6.3 μs after pulse (-○-); (c) e_{aq}^{-} in the presence of 0.5 M *tert*-butyl alcohol; N_2 saturated; 15 Gy; 0.2 μs; pH 6 (-●-) ([radical] = 4.1 μM); pH 14 (-■-) ([radical] = 4.6 μM).

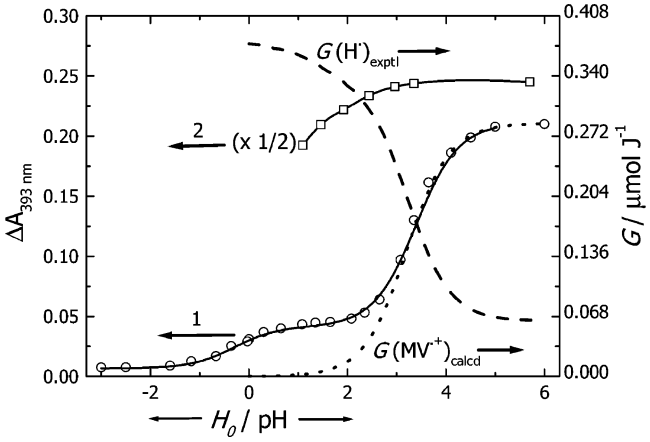

Figure 3. Absorbance (ΔA_{393}) vs solution acidity for e_{aq}^{-} assisted reduction of 200 μM MV^{2+} in the presence of 0.2 M *tert*-butyl alcohol under N_2 saturation; dose 15 Gy (-○-). Similar results obtained with $CO_2^{\bullet-}$ radical in the presence of additional 1.0 M (total of) HCO_2H and HCO_2^{-} under N_2 saturation (-□-). Yield of $H^{\bullet}$ radical (− − −) and e_{aq}^{-} (...) from Figure 1 are included for comparison.

Experimental Observations *vis-á-vis* Electron-Density Projections. The acidity-related after-pulse ΔA_{393nm} maximally obtained with N_2-saturated, 200 μM MV^{2+} and 0.2 M *tert*-butyl alcohol solution is plotted in Figure 3 (Curve 1). For comparison, $G(MV^{\bullet+})$ values are calculated from $G(e_{aq}^{-})$ using eq 11, taking into account the relative propensities of reactions 1 ($R = e_{aq}^{-}$) and 3 and are included in Figure 3 as $G(MV^{\bullet+})_{calcd}$. The $G(e_{aq}^{-})$ value used in eq 11 is equal to 0.28 μmol J^{-1}.

$$G(MV^{\bullet+})_{calcd} \approx G(e_{aq}^-) \times (k_1 \times [MV^{2+}])/(k_1 \times [MV^{2+}] + k_3 \times [10^{-pH}]) \quad (11)$$

$$G(H^\bullet)_{exptl} \approx G(e_{aq}^-) - G(MV^{\bullet+}) + G(H^\bullet) \quad (12)$$

Below pH 4, due to the increased scavenging of e_{aq}^- following reaction 3, availability of $[e_{aq}^-]$ for reaction with MV^{2+} decreases rapidly, lowering the yield of $MV^{\bullet+}$. However, instead of reaching a value of ~0 at pH ≤ 1, the experimental $G(MV^{\bullet+})$ value is found to become stabilized at ~0.055 μmol J^{-1} between pH 0.6−1.5. The complementary value of $G(H^\bullet)_{exptl}$, required later for relating with $G(MV^{\bullet+})$, is obtained from eq 12 and is included in Figure 3 for the sake of completeness. The quantity $G(H^\bullet)$ in eq 12 represents the pH dependent after pulse yield of $H^\bullet$.[32]

From Figure 3, the following conclusions are drawn. Close match of ΔA_{393nm} (Curve 1) and $G(MV^{\bullet+})$ values between pH 3−6 indicates that the $[MV^{\bullet+}]$ radical is not protonated (pK_a of 2.9) as suggested by Solar et al.[12a] and later rejected by Venturi et al.[12c] Absence of a transient pK_a value, even up to pH 1, is also evident from the plot of ΔA_{393nm} vs pH (Curve 2) in Figure 3, describing $MV^{\bullet+}$ generation by the $CO_2^{\bullet-}$ radical (reaction 10). Here the $G(MV^{\bullet+})$ values closely follow the $G(CO_2^{\bullet-})$ profile in this pH range; the continuous decrease in the latter below pH 3 takes place because of slower $CO_2^{\bullet-}$ radical generation from HCO_2H, as compared to HCO_2^- at higher pH as mentioned earlier. Below pH 3, the ΔA_{393nm} values (Curve 1) deviate from the $G(e_{aq}^-)$ profile.

An enlarged Curve 1 in Figure 4 shows that the variation in ΔA_{393nm} values below pH 3 matches well with a deprotonation relation defined by the Henderson equation and provides a transient pK_a value of −0.2. The pK_a value remains identical if the observed ΔA_{393nm} values are normalized for the variation in $G(H^\bullet)$ (comparing with the yield from Figure 1 for the acidity range covered). The radical deprotonation step is further supported by the kinetic traces shown in the Figure 4 inset. Herein, although the kinetic trace at H_0 −0.36 shows a continuous rise in absorbance ($\tau_{1/2} \approx 10$ μs), the trace at pH 1.65 shows a two-stage increase, first an after-pulse fast rise (due to a minor direct $e_{aq}^- + MV^{2+}$ reaction) and later a slower but matching rise ($\tau_{1/2} \approx 10$ μs) as above. At H_0 −0.36, because of negligible direct e_{aq}^- reaction with MV^{2+}, the slow ΔA_{393nm} rise confirms a subsequent radical reaction such as its deprotonation. A lower transient absorbance at H_0 −3.0 is commensurate with an unfavorable deprotonation reaction at higher acidity. At pH 1.65, the 35 μs after-pulse transient spectral profile closely matched the $MV^{\bullet+}$ spectrum. From comparisons of the maximum ΔA_{393nm} value and $G(H^\bullet)$, it is found that only ~14% of the H adducts give rise to the $MV^{\bullet+}$ species following reaction 13. It is to be noted that in these and all subsequent results, the fraction of the H atoms not reacting with MV^{2+} but getting scavenged by *tert*-butyl alcohol and also disappearing following its radical−radical reaction were accounted for.[6]

$$MVH^{\bullet 2+} + H_2O \leftrightarrow MV^{\bullet+} + H_3O^+ \quad (13)$$

Because the electron density values (vide Appendix) support preferential addition of H atoms onto one of the two N atoms in MV^{2+}, only one deprotonation step can originate from this adduct ($MVH_{N4}^{\bullet 2+}$) with concurrent formation of $MV^{\bullet+}$. (Deprotonation from the alternate addition site i.e., C2, would be implausible at this acidity because of the sp^3 nature of the host C atom in such an adduct.) Thus, the pK_a value of −0.2 measured above is proposed to represent the $MVH_{N4}^{\bullet 2+}$ deprotonation. As a corollary ~14% of H atoms attach to the N4 atom. Although the $MVH_{N4}^{\bullet 2+}$ species can be compared to a protonated tertiary ammonium species with the $-CH_3$ and cyclohexadienyl cationic radical substitutions on the N4 in addition to the hydrogen, its strong acidity probably arises from a combination of the following effects: (i) presence of the ring substituent possessing an unpaired spin, (ii) effect of substituent positive charge, increasing the electron deficiency on the N4 atom, and (iii) favorable hydration of the deprotonated, planar $MV^{\bullet+}$ radical with the concurrent reduction of structural strain.[33]

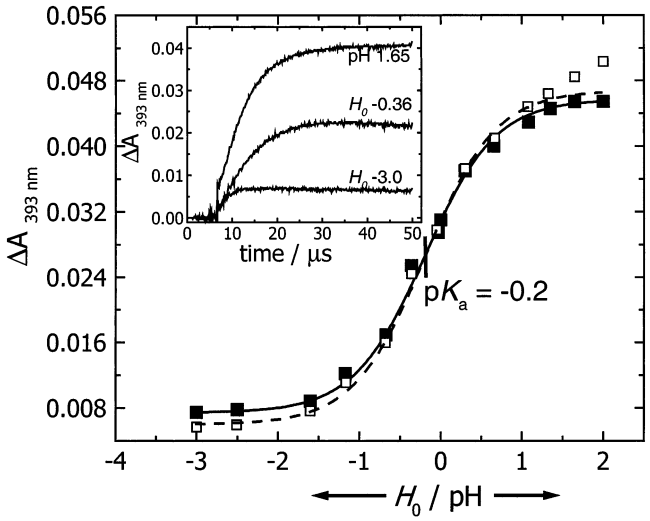

Figure 4. Radical pK_a obtained from experimental ΔA_{393} (-■-) vs acidity and also for normalized ΔA_{393} (-□-) under a uniform yield of $H^\bullet$ radical over the acidity range for conditions give in Figure 3. Inset: Growth of the transient absorption signal at a different solution acidity.

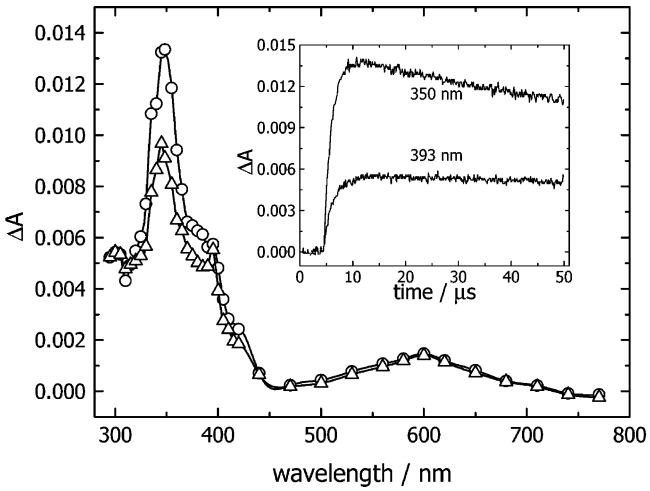

Figure 5. Time-resolved transient spectra obtained in N_2-saturated 340 μM MV^{2+} and 0.27 M *tert*-butyl alcohol at H_0 −1.7; dose 11 Gy, producing ~5 μM H atom. ΔA_{max} shown at 6 μs (-○-) and 38 μs (-△-) after end of pulse. Inset: Kinetic traces obtained at the two peak wavelengths.

Other Reactions of the H Atom. To understand the reaction pathway(s) followed by the remaining ~86% H atoms, spectral measurements were made in highly acidic N_2-saturated solutions. A new peak centered at 350 nm appeared below pH 0 with concurrent reduction of ΔA_{393nm} due to the $MV^{\bullet+}$ radical. The latter completely vanished at H_0 −3.0 as the 350 nm peak gained prominence. Time-resolved transient radical absorption spectra measured at an intermediate acidity (H_0 −1.7) is shown in Figure 5. A minor shoulder at 393 nm and the characteristic broad 605 nm peak reveals some finite contribution from the $MV^{\bullet+}$ radical. The Figure 5 inset indicates matching transient formation

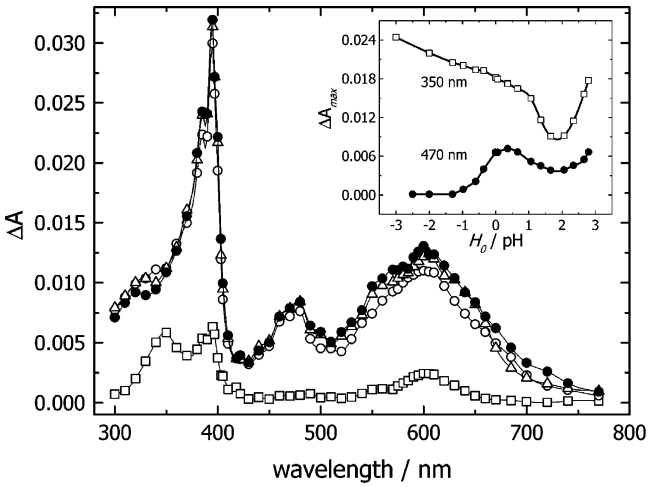

Figure 6. Time-resolved transient spectra obtained in N_2-saturated 200 μM MV^{2+} and 0.27 M *tert*-butyl alcohol solution at pH ~0.5; dose 15 Gy, producing 5.6 μM H atom. ΔA at 1.4 μs (-□-), 12.7 μs (-○-), 20 μs (-△-), and 38 μs (-●-) after end of pulse. Inset: Plot of ΔA_{max} vs acidity shown for comparison.

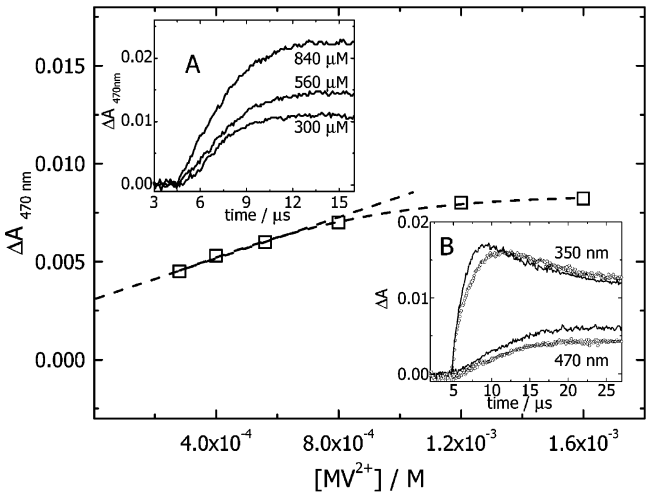

Figure 7. Variation of ΔA_{470nm} with increasing concentration of MV^{2+} in N_2-saturated pH ~0.5 solution in the presence of 0.1 M *tert*-butyl alcohol; dose 14 Gy. (Inset A) Comparison of transient formation kinetics at 470 nm with 44 Gy dose with 0.2 M *tert*-butyl alcohol and at different concentrations of MV^{2+}. (Inset B) Comparison of transient formation kinetics at 350 and 470 nm. Dose 14 Gy, 0.2 M *tert*-butyl alcohol, $[MV^{2+}] = 300$ μM and 650 μM (left, 350 nm and top, 470 nm) in either case.

kinetics at 350 and 393 nm with no further slow rise in the ΔA_{393nm}, as is expected at this acidity (in analysis of all radical formation kinetics, any radical decay therein was always taken into consideration). Different decay kinetics at 350/393 nm, however, confirms dissimilar nature of the two transients. While the transient decay measurements at 350 nm revealed a second-order kinetics, suggesting a radical−radical reaction, our attempt to check the effect of O_2 on this radical decay was not successful because of preferential scavenging of the H atom by O_2 forming the $HO_2^{\bullet}$ radical. To quantify the radical absorption characteristics, additional information regarding its yield was obtained from the following results.

In N_2-saturated MV^{2+} solution at pH ~0.5, the time-resolved spectra in Figure 6 reveal four peaks. Different formation kinetics of the peak absorptions at 350 and 470 nm suggests that if the former (as for 393 nm) arises because of a primary radical, then the latter is caused by a secondary radical. This is further rationalized below in Figure 7. The Figure 6 inset shows the change in ΔA_{max} at 350 and 470 nm with an increase in solution acidity. If the increase in transient absorbance at 350 nm with increasing acidity is related to the $G(H^{\bullet})$, it is found to remain proportional to the latter below pH 1.5. For these calculations, any contribution of the $MV^{\bullet+}$ radical absorption at 350 nm was taken into account (related to the absorbance at 605 nm). Above pH > 1.5, the masking effect of the 393 nm peak increased rapidly, preventing further quantitative estimation of the concerned radical absorbance at 350 nm. Above pH 4 it is expected that contribution to the total 350 nm absorbance from this peak would fall to a negligible level as $G(H^{\bullet})$ levels off to its limiting value and e_{aq}^- dominates MV^{2+} reduction. These results, however, suggest that at pH < 1.5 the transient species giving rise to the absorption peak at 350 nm does not deprotonate (verified up to H_0 −4.7).

In the pH range 0.4−1.2, measurements at 470 nm reveal the several characteristics of the concerned radical. (1) First-order rate of increase in ΔA (k_ϕ^f) is independent of $[MV^{2+}]$ but increases with the dose (i.e., starting H atom concentration). For example, kinetic traces obtained with a 44 Gy dose reveal a similar signal rise time of ~10 μs ($k_\phi^f = 2.1 \pm 0.2 \times 10^5$ s^{-1}, Figure 7, inset A), whereas with a 14 Gy dose the corresponding values (Figure 7, inset B) are ~18 μs ($1.0 \pm 0.1 \times 10^5$ s^{-1}). On the other hand, the kinetics at 350 nm is significantly faster. At a 14 Gy dose it reaches its maximum value within ~5 μs at 300 μM MV^{2+} and in ~3.5 μs at 650 μM MV^{2+} (Figure 7, inset B) and therefore reconfirms the earlier proposition that the concerned radical forms directly in a H atom reaction with MV^{2+}. Irrespective of the dose (14 or 44 Gy), the ΔA_{470nm} decay followed a complex kinetics, although a segment of the respective kinetic traces could be analyzed for a second-order decay (with $2k/\epsilon$ value $= 1.9 \pm 0.3 \times 10^6$ M^{-1} s^{-1}). (2) The increase in ΔA_{470nm} maximum value with increasing $[MV^{2+}]$ takes place with concurrent increase in the values of $\Delta A_{350/393/605nm}$. (3) The linear increase in ΔA_{470nm} with $[MV^{2+}]$ (Figure 7) below millimolar concentration slowly levels off above it. The profiles of ΔA vs $[MV^{2+}]$ at 350/393/605 nm plots remain similar. When these measurements were repeated with higher concentrations of *tert*-butyl alcohol (up to 0.6 M), but maintaining ≥0.8 reactivity of the H atom toward MV^{2+}, no qualitative differences were noticed in these characteristics. These observations imply that, unlike in the 350 nm case, the concerned species with its λ_{max} at 470 nm forms only in a secondary reaction, most certainly from another H atom-generated radical. Time-resolved spectral measurements from 300 to 800 nm made to trace this intermediate species, however, remained unsuccessful. Continuing with our earlier discussion of the reaction possibilities, the remaining two, i.e., (i) ring addition at C2 and (ii) methyl H atom abstraction seem most likely to be responsible for the two transients giving rise to absorption peaks at 350 and 470 nm. For quantitative correlation, additional results from the $^{\bullet}OH/^{\bullet}O^-$ + MV^{2+} reactions were needed.

Transients Formed in $^{\bullet}OH/^{\bullet}O^-$ Reactions with MV^{2+}. Time-resolved absorption spectra in Figure 8 are obtained from the $^{\bullet}OH$ radical reaction with MV^{2+}. The three peaks centered at 393, 470, and 605 nm matched with the results of similar measurements in the past.[18,34] When measurements were extended up to 290 nm, another peak at 315 nm was also recorded in the present work. Detailed kinetic analyses at each of these peak wavelengths reveal some new information. As shown in the Figure 8 inset, the kinetic traces indicate the presence of only two types of transient species. The after-pulse sharp rise at 393/605 nm peaks in all certainty refer to the $MV^{\bullet+}$ species as discussed before, formed by a direct reaction of ~11% e_{aq}^- with MV^{2+} as compared to the scavenging of the remaining

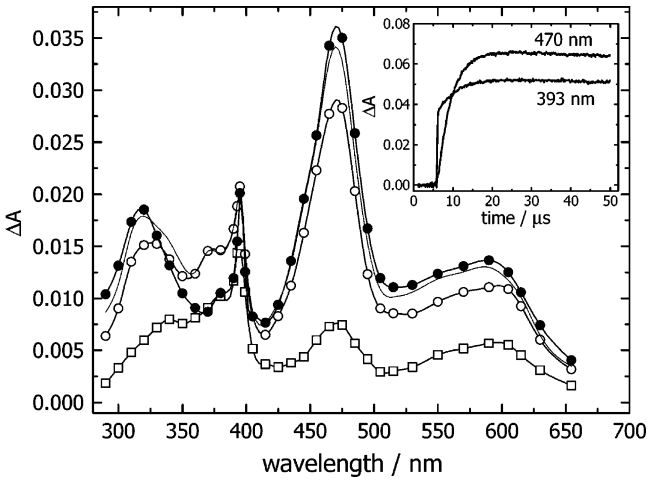

Figure 8. Time-resolved transient spectra obtained with N_2O-saturated 250 μM MV^{2+} solution at pH ~6.0; dose 15 Gy, generating ~8.5 μM total radical concentration. ΔA at 1.5 μs (-□-), 8.0 μs (-○-), 13 μs (-●-), and 40 μs (—) after end of pulse. Inset: Transient formation kinetics at different peak wavelengths for comparison.

e_{aq}^- by N_2O following reaction 6. (Additionally, a small contribution toward $\Delta A_{393/605nm}$ is expected because of the deprotonation of ~14% in all $MVH_{N4}^{\bullet 2+}$ species with $G = 0.0074$ μM J^{-1} from the H atom reaction.) The increase of ΔA_{315nm} is comparatively slower than the after-pulse sharp rise of $\Delta A_{393/605nm}$, but its time scale matches with the ΔA_{470nm} kinetics. At a low dose of ~5 Gy, the bimolecular rate constant of transient formation at 315/470 nm was estimated, from the kinetic traces at varying concentrations of MV^{2+}, to have a value of $1.9 \pm 0.3 \times 10^8$ M^{-1} s^{-1}, matching a previous estimate of 2.0×10^8 M^{-1} s^{-1}.[18] Even at 393/605 nm, the second, slower rate of increase in absorbance matched the increase in $\Delta A_{315/470nm}$, suggesting that this increase was mainly due to the tailing effects of the transient absorption peaks at 315/470 nm. Although no attempt was made to separate the absorption spectral profile of the transient from $^{\bullet}OH$ radical reaction from that of $MV^{\bullet +}$ absorption, the direct yield of the $MV^{\bullet +}$ transient was obtained as follows. Assuming negligible loss of e_{aq}^- by radical−radical reactions, the radical yield (in μM) for a few 100 μM MV^{2+} concentrations was calculated from eq 14.

$$G(MV^{\bullet +}) \approx 0.28 \times \{[MV^{2+}] \times 9.0 \times 10^{10}\}/\{[MV^{2+}] \times 9.0 \times 10^{10} + 0.025 \times 9.1 \times 10^9\} \times D \quad (14)$$

In eq 14, the numerical value 0.28 represents the $G(e_{aq}^-)$ in μM J^{-1}; 9.0×10^{10} represents k in the $MV^{2+} + e_{aq}^-$ reaction; 0.025 represents the saturated molar N_2O concentration in water at 26 °C; 9.1×10^9 represents k in the $N_2O + e_{aq}^-$ reaction; and D represents the dose in Gy. Subsequently, from the previously obtained ratios of $MV^{\bullet +}$ and ΔA values for 393/315, 393/470, and 605/470 nm, the ΔA values at 315/470 nm for the $^{\bullet}OH$ radical reaction transient were obtained.

Since the results of electron-density calculations on the parent MV^{2+} (vide Appendix) indicate an excess electron density on both the N atoms, the electrophilic nature of the $^{\bullet}OH$ radical hints that one of these two N atoms is the preferred site of addition. The relevant $^{\bullet}OH$ radical reactions are shown in Scheme 2. The $^{\bullet}OH$ radical attachment on the N4 atom directly produces the radical R2. A comparison of excess electron-charge values on N4 with C2 or other ring C atoms (vide Appendix) suggests that addition of an $^{\bullet}OH$ radical would be preferred only at N4. As detailed investigation of the transient absorption

SCHEME 2

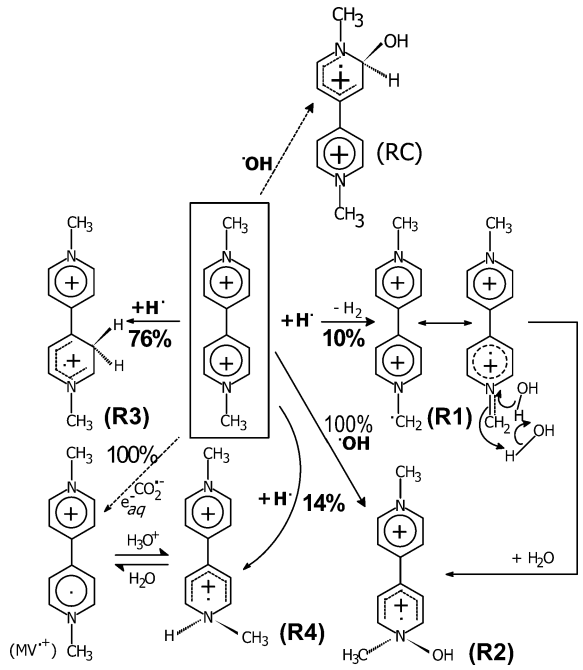

spectrum, as well as decay kinetics, suggests formation of only one transient, it is proposed that only radical R2 is formed as a result of $^{\bullet}OH$ radical reaction. At MV^{2+} concentration >1 mM, propensity of reaction 1 or reactions 6/7 is almost equal. Therefore, as proposed earlier,[35] spur scavenging of e_{aq}^- can take place both by MV^{2+} and N_2O to equal extent. The total yield of the oxidized radical in N_2O-saturated solution, at a 14 Gy dose and an experimental MV^{2+} concentration of ca. 1.6 mM, is thus estimated at ~0.445 μmol J^{-1}, taking ~90% efficiency of reaction of $^{\bullet}OH$ radicals with MV^{2+} while the rest are lost in other radical reactions. Then, from the transient ΔA_{max} values obtained in experiments employing 1.0−3.0 mM MV^{2+}, ϵ(R2) values are estimated as $15\,300 \pm 700$ M^{-1} cm^{-1} at λ_{max} 470 nm; 7400 ± 400 at 315 nm; 2000 ± 250 at 393 nm, and 1620 ± 200 at 605 nm. From the measured after-pulse ΔA_{max} values at 393/605 nm, the interference of the $MV^{\bullet +}$ absorption at these wavelengths were estimated, and the above ϵ(R2) values have been presented after due correction. The ϵ(R2) value at 470 nm is close to the value of 16 000 M^{-1} cm^{-1} proposed by Solar et al.[34] The ϵ_{470nm} value is mandatory for a final quantification of the $H^{\bullet}$ reaction pathways in the next section.

In the earlier study dealing with $^{\bullet}OH$ radical reactions with MV^{2+},[34] a transient pK_a value of 9.7 was observed that can now be explained on the basis of the cyclohexadienyl radical structure of R2 incorporating the hydroxy-substitution on the sp^3, cationic ring nitrogen ($MVOH_{N4}^{\bullet 2+}$). In comparison, if OH addition takes place on another atom, say C3, the radical RC ($MVOH_{C3}^{\bullet 2+}$) would result. Analysis of the concerned physical parameters (vide Appendix Table 3) reveals a possibility of radical R2 (N)O−H group deprotonation at mildly alkaline pH. On the other hand, a similar deprotonation of the (C)O−H group attached to the sp^3 C3 atom in radical RC seems to be possible only at a higher pH.

In oxidation studies employing the $^{\bullet}O^-$ radical at pH ≈ 14, entirely different results are obtained. As shown in Figure 9, apparently only the semi-reduced transient $MV^{\bullet +}$ spectrum is obtained irrespective of the nature of the gas used for purging the solutions, i.e., N_2 or N_2O, wherein reactions 15−17 also take place.

$$^{\bullet}OH + OH^{-} \leftrightarrow {}^{\bullet}O^{-} + H_2O \ (pK_a\ 11.9) \quad (15)$$

$$HO_2^{-} + {}^{\bullet}OH \rightarrow O_2^{\bullet -} + H_2O \quad (16)$$

$$HO_2^{-} + {}^{\bullet}O^{-} \rightarrow O_2^{\bullet -} + OH^{-} \quad (17)$$

All the H_2O_2 formed from irradiation is expected to deprotonate at pH $\approx$ 14 and exist as HO_2^- ($pK_a = 11.7$). At pH $\approx$ 14, >99% $^{\bullet}OH$ radicals exist as $^{\bullet}O^-$. Because the $MV^{\bullet +}$ species is a stronger reducing agent than $O_2^{\bullet -}$,[10] the propensity of reaction 18 is expected to be low. An earlier estimate of $k_{18} = 1 \times 10^4\ M^{-1}\ s^{-1}$ is available in the literature based on the reduction potentials and the reverse reaction rate.[36]

$$O_2^{\bullet -} + MV^{2+} \rightarrow O_2 + MV^{\bullet +} \quad (18)$$

The kinetic traces in N_2-saturated solution in the Figure 9 inset show a two-stage increase in the absorbance. In this case, the immediate after-pulse increase in $\Delta A_{393/605nm}$ arises because of the direct reaction of MV^{2+} with e_{aq}^- and closely follows the calculated yield of $MV^{\bullet +}$, while the subsequent second-stage increase in absorbance suggests further reduction of MV^{2+}. The slower second-stage $MV^{\bullet +}$ formation kinetics in N_2-saturated solution or its direct formation in N_2O-saturated solution follows a first-order kinetics, and the observed rate remains within the range $2.3 \pm 0.3 \times 10^5\ s^{-1}$. Because this observed rate remains unexplained by any published rate value, reaction 19 with the $^{\bullet}O^-$ radical in the presence of such high concentrations of OH^- is proposed as a possible route of $MV^{\bullet +}$ generation via the adduct $[MV\text{- -}O]^{\bullet +}$ formation.

$$MV^{2+} + {}^{\bullet}O^{-} \rightarrow [MV\text{- -}O]^{\bullet +} - (OH^{-}) \rightarrow MV^{\bullet +} + HO_2^{-} \quad (19)$$

However, it may be noted that these $^{\bullet}O^-$ reactions or results have no direct correlation in our present studies, and further experiments in this direction were not attempted.

MV^{2+} Reaction with H Atom Revisited. Continuing with the H atom reactions with MV^{2+}, the H abstraction reaction is seen to result in the formation of the radical R1 (Scheme 2). Although radical R1 can be partially resonance stabilized, as suggested by a decrease of 0.1 in the N−C bond order for the $>N-CH_2^{\bullet}$ group as compared to that of the $>N-CH_3$ group in the parent, its optical absorption in the visible region is suggested to be low.[12a,b] Among various possibilities, radical R1 can decay by (1) an intramolecular rearrangement, (2) reaction with another radical (R1 included), (3) reaction with solvent. Taking into account all the results obtained at 470 nm from both the H atom and $^{\bullet}OH$ radical studies, we envisaged the mechanism shown in Scheme 2 for generation of radical R2 from R1 in aqueous medium. Further support for this mechanism is derived from the following observations. Although intramolecular rearrangement of radical R1 or its subsequent reaction with solvent (H_2O) would follow a first-order rate, the dose dependency observed before eliminates the former possibility. On the other hand, the latter mechanism also supports the observations of the rate remaining independent of $[MV^{2+}]$ but depending on the dose, i.e., G(R1). The dependence of ΔA_{470nm} on $[MV^{2+}]$ shown in Figure 7 also eliminates the second possibility of a radical−radical reaction. The nature of the plot is explained on the basis of a general increase in propensity of radical−solute reactions leading to a higher yield of its precursor radical R1. Nondependence of these results on [*tert*-butyl alcohol] also eliminates any possibility of its involvement. From the measured ΔA_{470nm} and ϵ_{470nm} values in the H atom and $^{\bullet}OH$ radical studies, respectively, G(R2) is found to be ~10% of $G(H^{\bullet})$.

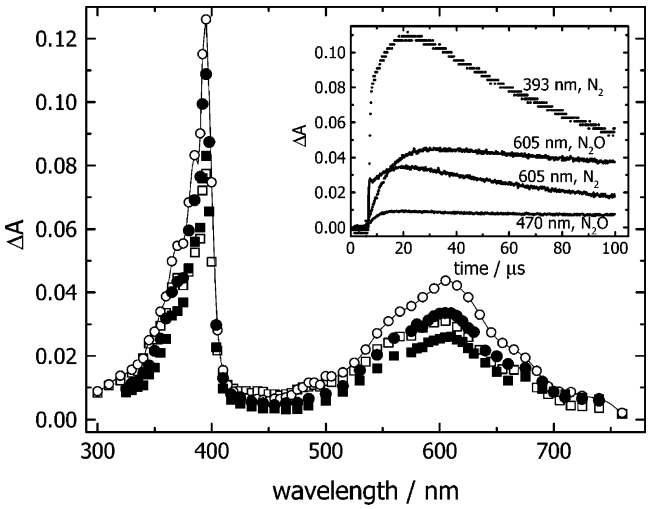

Figure 9. Time-resolved transient spectra obtained with N_2O-saturated 60 μM MV^{2+} solution at pH ~14.0; dose 8 Gy, generating ~5.2 μM total radical concentration. ΔA at 9 μs (-□-), 30 μs (-○-), 42 μs (-●-), and 85 μs (-■-) after end of pulse. Inset: Transient formation kinetics at different peak wavelengths under N_2 or N_2O saturation.

Our earlier observation in the Figure 6 inset regarding the decreasing transient absorption at 470 nm at pH < 0 and pH > 1 is explained below. In acidic solutions (H_0 < 0), higher concentration of H_3O^+ may directly compete with the H_2O addition step and consequently allow radical R1 to decay by other routes or indirectly affect the radical R2 absorbance by a protonation step i.e., reduce its visibility. On the other hand, in solutions of lower acidity, because of rapidly reducing $G(H^{\bullet})$, the radical R2 absorption is expected to decrease and its weak absorption to become masked under the more intense absorption profile of the $MV^{\bullet +}$ species. Only near pH range 0−1, as the influence of the $MV^{\bullet +}$ species becomes negligible, does the 470 nm peak due to radical R2 remain visible.

The overall H atom reaction rate constant ($k_{H^{\bullet}+MV^{2+}}$) was estimated separately from the rates of growth of transient absorption at 350/393 nm in appropriate solutions. The estimated value ($6.4 \pm 0.7 \times 10^8\ M^{-1}\ s^{-1}$) is close to the previously reported value of $6.0 \times 10^8\ M^{-1}\ s^{-1}$.[12a] The 350 nm peak is now expected to arise from the remaining possibility, i.e., the $MVH_{C2}^{\bullet 2+}$ radical (Radical R3, Scheme 2), and its yield is found to be ~76% of $G(H^{\bullet})$. After accounting for the actual concentration of H atoms generating the radical R3 and with due correction of the ΔA_{350nm} value, taking into account any contribution of the $MV^{\bullet +}$ radical, the ϵ_{350} value is calculated as $4470 \pm 300\ M^{-1}\ cm^{-1}$ (peak absorption 350 nm, fwhm = 40 nm) leading to the second-order decay rate $2k_{350nm} = 2.6 \pm 1.1 \times 10^9\ M^{-1}\ s^{-1}$, for a possible radical−radical-type reaction.

Conclusions

The mechanism of H atom reaction with MV^{2+} has been derived from pulse radiolysis measurements in $HClO_4$ solution and is supported by ab initio MO calculations. Scheme 2 shows the relevant results from this study for easy reference. It is found that only ~14% of all the H atom reaction leads to the formation of the H adduct at N4 (radical R4). The pK_a for this H adduct has been estimated to be −0.2. On deprotonation at an appropriate solution pH, it produces the semi-reduced species $MV^{\bullet +}$. A comparison of MV^{2+} reactions with a H atom and a

•OH radical shows that only 10% of the H atom reactions are estimated to abstract a hydrogen from the $>N-CH_3$ group, generating the radical R2 in aqueous solution through the intermediacy of the radical R1. MO calculations support a deprotonation of the (N)O−H group in mildly alkaline medium, thus supporting a pK_a value of 9.7 observed earlier.[34] Radical R2 decay at 470 nm follows complex kinetics, suggesting more than one decay channel. The majority of H atom reactions (76%) proceeds via its addition to the ring C2 atom, generating the radical R3. The latter decays following a radical−radical reaction imply concurrent loss of the parent molecule. However, if this reaction can regenerate the parent (and simultaneously the dihydro species in a disproportionation reaction) as proposed in a similar study on 4,4′-bipyridyl,[37] then the parent recovery would be ∼38% following this reaction. The total parent recovery can thus rise to a maximum value of ∼52% if we assume complete recovery from the $MV^{\bullet+}$ species discussed above. Therefore, in systems where the reversibility of the $MV^{2+}/MV^{\bullet+}$ couple is employed as in the color displays, avoidance of the H atom in the system would be essential for a longer system life. Academically, the R4 radical generation suggests a correction factor of ∼0.008 μmol J^{-1} for $MV^{\bullet+}$ yield in pulse radiolysis measurements in mildly acidic or alkaline pH. In the present study, the importance of proper placement of the dipositive charge to assess the electrophilic attachments of the H atom and the •OH radical and appropriate selection of the experimental acidity are highlighted.

Acknowledgment. We thank our colleagues Mr. Vijendra N. Rao and Drs. Sambhu N. Guha and Tulsi Mukherjee for the support during this study and the reviewers for their valuable suggestions.

Appendix

The numerical values were obtained by employing ab initio MO methods, namely, Hartree−Fock (HF) with 6-31G* basis set dealing with structure and electron and spin density (for radicals discussed later) mappings for the respective species using the GAMESS software package for calculations.[21] The relevant atom-in-molecule electron populations as well as the (radical) spin populations were obtained using the Mulliken population analysis scheme for net charge/spin at the atomic sites. Relevant details for parent MV^{2+} are shown in Table 1.

In the geometry-optimized configuration (dihedral angle ∼49° between the two rings), contrary to the general representation in the literature, each of the two N atoms possess an excess charge of 0.590e such as the C2/C6/C8/C12 atoms (all equivalent, each possess ∼0.268e additional charge) and C21/C22 atoms (each possess additional 0.342e charge). The charge deficiency is mainly shared by the C1/C7 atoms (0.078e each), C3/C5/C9/C11 atoms (av 0.177e each), and all the H atoms.

Projections for $MV^{\bullet+}$ Transient. Calculations for the $MV^{\bullet+}$ species show that in its geometry-optimized configuration the two rings are coplanar (dihedral angle ∼0°). In this case, the additional negative charge as compared to MV^{2+} gets distributed on N4/N10 (increase marginally by 0.050e each) and C2/C6/C8/C12 (increase by 0.022e). Similarly, the charge deficiency at C1/C3/C5/C7/C9/C11 is reduced by 0.025e−0.033e. The remaining electron charge in $MV^{\bullet+}$ mainly gets distributed to the H atoms; however, the charge of both C21/C22 atoms shows a marginal lowering by 0.030e.

The spin density values in $MV^{\bullet+}$ are highest on the two bridging C1 and C7 atoms (0.2 each), whereas the remaining 0.6 is mainly distributed over N4 and N10 (0.076 each), C2/C6/C8/C12, and C3/C5/C9/C11 (∼0.054 each). While these integrated spin-density values provide the clue for subsequent $MV^{\bullet+}$ radical−radical reaction channels, the relative net atomic charge values help in assessing the relative ease of a proton addition (at a suitable acidic pH) on different C/N atoms in $MV^{\bullet+}$ rings. The results suggest possible protonation at N4 and C2 atoms.

TABLE 1. MV^{2+} Atomic Charge and Bond Distance/Order

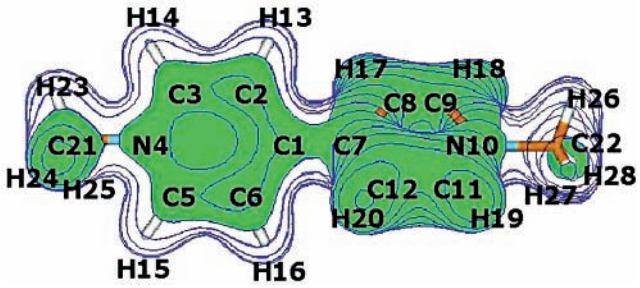

atom	net charge	atom	net charge	atom	net charge
N4	−0.590	C8	−0.267	H16	0.302
N10	−0.590	C5	0.175	H18	0.322
C3	0.179	C9	0.175	C21	−0.342
C11	0.179	H13	0.302	C22	−0.342
C2	−0.269	H20	0.302	H23	0.255
C12	−0.269	H14	0.322	H24	0.266
C1	0.078	H15	0.323	H25	0.266
C7	0.078	H19	0.323	H26	0.255
C6	−0.267	H17	0.302	H27	0.266
				H28	0.266

atom pair		distance	bond order	atom pair		distance	bond order
4	3	1.334	1.196	1	2	1.390	1.418
4	5	1.338	1.175	7	12	1.390	1.417
4	21	1.490	0.756	5	6	1.372	1.498
10	9	1.338	1.175	2	13	1.073	0.890
10	11	1.334	1.195	12	11	1.377	1.466
10	22	1.490	0.756	12	20	1.073	0.890
3	2	1.377	1.465	5	15	1.073	0.887
3	14	1.072	0.885	11	19	1.072	0.885
9	8	1.373	1.497	22	26	1.077	0.930
9	18	1.073	0.887	22	27	1.079	0.919
6	1	1.394	1.393	22	28	1.079	0.919
6	16	1.073	0.889	21	23	1.077	0.930
8	7	1.394	1.393	21	24	1.079	0.919
8	17	1.073	0.889	21	25	1.079	0.919
1	7	1.495	1.031				

Projections for MV^{2+} + H• Reaction Transients. In the case of H addition, the adduct species is expected to have four possible structures relative to the different sites of H addition, represented as $MVH_A^{\bullet 2+}$, where the subscript A represents the site of H addition, i.e., C1, C2, C3, or N4 atoms. In case of such addition and also for methyl−H abstraction reaction, the resulting radical stability, dipole moment, atomic electron, and spin-density distributions allow a comparison of the relative propensities of the different H atom reaction channels. In all cases of H addition, a reduction in conjugation and increase in radical dipole moment is obtained. In the present set of calculations, first a low-level calculation (HF/STO-3G) was performed for the $MVH_A^{\bullet 2+}$ species in the gas phase. A subsequent high-level calculation (HF/631-G*) in the gas phase in each case showed insignificant change with respect to the values obtained in low-level calculations.

From MV^{2+} properties the following qualitative inferences can be drawn: (1) an electrophilic addition of H atom on N4 is most favored, (2) its addition to only the C2 equivalent site is

TABLE 2. $MVH^{\bullet 2+}$ Adduct Properties

$MVH^{\bullet 2+}$ adduct	dihedral angle (deg)	dipole moment (D)
C1	~68	1.23
C2	~2	3.10
C3	~39	2.14
N4	~25	4.04

TABLE 3. $MVOH^{\bullet 2+}$ Adduct Properties

$MVOH^{\bullet 2+}$ adduct	dihedral angle (deg)	X−O bond order	O−H bond order	O atom electron density	H atom electron density
C3	~39	X = C3, 0.997	0.922	−0.260e	0.231e
N4	~28	X = N4, 0.919	0.911	−0.113e	0.262e

next-favored, and (3) calculated radical stability values also suggest the significant probability of H abstraction from a methyl group (−570 kcal mol^{-1} as compared to the average H adduct value ~−564 kcal mol^{-1}). In the case of N4 addition, one unit of electron spin is introduced in the resulting tertiary ammonium structure of $MVH_{N4}^{\bullet 2+}$, and its electron-density distribution pattern with respect to the MV^{2+} values changes as follows. The charge on C3/C5 reduces by 0.050e each, on N4 it reduces to 0.220e, and on C2/C6 it reduces considerably to 0.036e each. The integrated spin density on C3/C5 becomes 0.1 each and on C1 it becomes 0.68. As a result of the combined effect of the electron-charge deficiency and introduction of integrated spin density in the concerned ring, the atomic charge value on the N−hydrogen is reduced (from an ideal value of 1) by 0.313e and the N−H bond order becomes 0.865e. These values indicate that the pK_a value corresponding to the N−hydrogen deprotonation would have a value lower than the one normally reported for tertiary ammonium structures (i.e., 3−5).[38] On the other hand, if a comparative study of C2 atom protonation of $MV^{\bullet +}$ species is considered, it leads to the following results. The extra electron charges on respective atoms in the ring are as follows: N4 0.17e, C3 −0.21e, C2 0.125e, C1 −0.066e, C6 0.04e, and C5 −0.062e. The respective integrated atomic spin-density values are 0.001, 0.0118, 0.001, 0.731, 0.001, and 0.116. A comparison of the electron charge values on the two H atoms on C2 shows a deficiency of 0.137e each (from an ideal value of 1) and the respective bond orders are 0.939 each. Thus, acidity of any C2 hydrogen is expected to be low, and deprotonation in such a case is expected to take place only in highly alkaline pH. Table 2 shows $MVH^{\bullet 2+}$ adduct values.

Because of the near planarity of the two rings, resonance delocalization of charge would be maximum in the C2 adduct, followed by the N4 adduct. Dipole moment values also suggest favorable solvation for N4 and C2 adducts in aqueous solution as compared to the C3 and C1 adducts. Thus, starting either with the protonation of $MV^{\bullet +}$ species or from a comparison of the relative stability of different $MVH^{\bullet 2+}$ adducts formed, the most favored H addition sites in MV^{2+} are the C2 and the N4 atoms.

Projections for MV^{2+} + $^{\bullet}OH$ Reaction Transients. The relevant results are presented in Table 3 where the N4 adduct is compared with the C3 adduct, taking it as the representative of all the other C atom cases. Comparison of the relevant parameters suggests deprotonation from the (N)O−H group at a lower pH than from the (C)O−H on an sp^3 C atom.

References and Notes

(1) (a) Bus, J. S.; Aust, S. D.; Gibson, J. E. *Biochem. Biophys. Res. Commun.* **1974**, *58*, 749. (b) Bird, C. L.; Kuhn, A. T. *Chem. Sci. Rev.* **1981**, *10*, 49.

(2) Autor, A. P. *Life Sci.* **1974**, *14*, 1309.

(3) Homer, R. F.; Mees, G. C.; Tomlinson, T. E. *J. Sci. Food Agric.* **1960**, *11*, 309.

(4) Kelly, L. A.; Rodgers, M. A. J. *J. Phys. Chem.* **1994**, *98*, 6377.

(5) Koshechko, V. G.; Kiprianova, L. A.; Fileleeva, L. I. *Tetrahedron Lett.* **1993**, *33*, 6677.

(6) Ross, A. B.; Bielski, B. H. J.; Buxton, G. V.; Greenstock, C. L.; Helman, W. P.; Huie, R. E.; Grodkowski, J.; Neta, P.; Mallard, W. G. *NDRL-NIST Solution Kinetics Database*, version 3; National Institute of Standards and Technology: Gaithersburg, Maryland, 1994.

(7) (a) Derwent, J. R. *J. Chem. Soc., Chem. Commun.* **1980**, 805. (b) Crutchley, R. J.; Lever, A. B. P. *J. Am. Chem. Soc.* **1980**, *102*, 7129. (c) Okura, I.; Kim-Thuan, N. *J. Chem. Soc., Faraday Trans. 1*, **1981**, *77*, 1411. (d) Harriman, A.; Porter, G.; Richoux, M.-C. *J. Chem. Soc., Faraday Trans. 2*, **1981**, *77*, 833. (e) *Photochemical Conversion and Storage of Solar Energy*, Rabani, J., Ed.; Weizman: Jerusalem, 1982.

(8) Cummins, D.; Boschloo, G.; Ryan, M.; Corr, D.; Rao, S. N.; Fitzmaurice, D. *J. Phys. Chem. B* **2000**, *104*, 11449.

(9) Grätzel, M. *Nature* **2001**, *409*, 575.

(10) Wardman, P. *J. Phys. Chem. Ref. Data* **1989**, *18*, 1637.

(11) (a) Allen, A. O.; Hochanadel, C. J.; Ghormley, J. A.; Davis, T. W. *J. Phys. Chem.* **1952**, *56*, 575. (b) Baulch, D. L.; Cobos, C. J.; Cox, R. A.; Esser, C.; Frank, P.; Just, Th.; Kerr, J. A.; Pilling, M. J.; Troe, J.; Walker, R. W.; Warnatz, J. *J. Phys. Chem. Ref. Data*, **1992**, *21*, 411. (c) Anderson, A. R.; Hart, E. J. *J. Phys. Chem.* **1961**, *65*, 804. (d) Czapski, G.; Jortner, J.; Stein, G. *J. Phys. Chem.* **1961**, *65*, 956. (e) Hayon, E.; Allen, A. O. *J. Phys. Chem.* **1961**, *65*, 2181. (f) Jortner, J.; Rabani, J. *J. Am. Chem. Soc.* **1961**, *83*, 4868. (g) Jortner, J.; Rabani, J. *J. Phys. Chem.* **1962**, *66*, 2081. (h) Dixon, R. S. *Radiat. Res. Rev.* **2**, *237*, 1970. (i) Ghormley, J. A.; Stewart, A. C. *J. Am. Chem Soc.* **1956**, *78*, 2934. (j) Dorfman, L. M. *Science* **1963**, *141*, 493. (k) Hart, E. J. *Annu. Rev. Nucl. Sci.* **1965**, *15*, 125. (l) Allen, A. O. *Radiation Chemistry of Water and Aqueous Solutions*; Van Nostrand: Princeton, New Jersey, 1961.

(12) (a) Solar, S.; Solar, W.; Getoff, N.; Holcman, J.; Sehested, K. *J. Chem. Soc., Faraday Trans.* **1982**, *78*, 2467. (b) *J. Chem. Soc., Faraday Trans.* **1984**, *80*, 2929. (c) Venturi, M.; Mulazzani, Q. G.; Hoffman, M. Z. *Radiat. Phys. Chem.* **1984**, *23*, 229.

(13) Farrington, J. A.; Ebert, M.; Land, E. J.; Fletcher, K. *Biochim. Biophys. Acta* **1973**, *314*, 372.

(14) Krasna, A. I. *Photochem. Photobiol.* **1980**, *31*, 75.

(15) Watanabe, T.; Honda, K. *J. Phys. Chem.* **1982**, *86*, 2617.

(16) Meisel, D.; Mulac, W. A.; Matheson, M. S. *J. Phys. Chem.* **1981**, *85*, 179.

(17) Kosower, E. M.; Cotter, J. L. *J. Am. Chem. Soc.* **1964**, *86*, 5524.

(18) Patterson, L. K.; Small, R. D., Jr.; Scaiano, J. C. *Radiat Res.* **1977**, *72*, 218.

(19) Farrington, J. A.; Ebert, M.; Land, E. J. *J. Chem. Soc., Faraday Trans. 1* **1968**, *74*, 665.

(20) (a) Domae, M.; Katsumura, Y.; Jiang, P. Y.; Nagaishi, R.; Ishigure, K.; Kozawa, T.; Yoshida, Y. *J. Chem. Soc., Faraday Trans.* **1996**, *92*, 2245. (b) Domae, M.; Katsumura, Y.; Ishigure, K.; Byakov, V. M. *Radiat. Phys. Chem.* **1996**, *48*, 487.

(21) Schmidt, M. W.; Baldridge, K. K.; Boatz, J. A.; Elbert, S. T.; Gordon, M. S.; Jensen, J. H.; Koseki, S.; Matsunaga, N.; Nguyen, K. A.; Su, S. J.; Windus, T. L.; Dupuis, M.; Montgomery, J. A. *J. Comput. Chem.* **1993**, *14*, 1347.

(22) Guha, S. N.; Moorthy, P. N.; Kishore, K.; Naik, D. B.; Rao, K. N. *Proc. - Indian Acad. Sci., Chem. Sci.* **1987**, *99*, 261.

(23) Das, T. N. *J. Phys. Chem. A* **2001**, *105*, 9142.

(24) Buxton, G. V.; Stuart, C. R. *J. Chem. Soc., Faraday Trans.* **1995**, *91*, 279.

(25) Buxton, G. V.; Greenstock, C. L.; Helman, W. P.; Ross, A. B. *J. Phys. Chem. Ref. Data* **1988**, *17*, 513.

(26) Yates, K.; Wai, H. *J. Am. Chem. Soc.* **1964**, *86*, 5408.

(27) Swallow, A. J.; Inokuti, M. *Radiat. Phys. Chem.* **1988**, *32*, 185.

(28) Sehested, K.; Hart, E. J. *J. Phys. Chem.* **1975**, *79*, 1639.

(29) Simic, M.; Neta, P.; Hayon, E. *J. Phys. Chem.* **1969**, *73*, 3794.

(30) Neta, P.; Schuler, R. H. *J. Phys. Chem.* **1975**, *79*, 1.

(31) Jeevarajan, A. S.; Carmichael, I.; Fessenden, R. W. *J. Phys. Chem.* **1990**, *94*, 1372.

(32) Spinks, J. W. T.; Wood, R. J. *An Introduction to Radiation Chemistry*, 3rd ed.; Wiley-Interscience, Wiley & Sons: New York, 1990; Figure 6.1, p 262.

(33) March, J. *Advanced Organic Chemistry*, 4th ed.; Wiley & Sons: New York, 1992; p 270.

(34) Solar, S.; Solar, W.; Getoff, N.; Holcman J.; Sehested, K. *J. Chem. Soc., Faraday Trans. 1* **1985**, *81*, 1101.

(35) Schuler, R. H.; Hartzell, A. L.; Behar, B. *J. Phys. Chem.* **1981**, *85*, 192.

(36) Tsukahara, K.; Wilkins, R. G. *J. Am. Chem. Soc.* **1985**, *107*, 2632.

(37) Buntinx, G.; Valat, P.; Wintgens, V.; Poizat, O. *J. Phys. Chem.* **1991**, *95*, 9347.

(38) Tables 8-1 in reference 33.